Chemical Geology 591 (2022) 120718

Contents lists available at ScienceDirect

Chemical Geology

journal homepage: www.elsevier.com/locate/chemgeo

Effects of salinity on the leaching of ionic species from hydrocarbon target formations during hydraulic fracturing

Katherine N. Snihur [a,*], Logan R. Swaren [a], Konstantin von Gunten [a], Nicholas B. Harris [a], Siobhan A. Wilson [a], Murray K. Gingras [a], Kurt O. Konhauser [a], Shannon L. Flynn [b], Daniel S. Alessi [a]

[a] Department of Earth and Atmospheric Sciences, University of Alberta, Edmonton, AB T6G 2E3, Canada
[b] School of Natural and Environmental Sciences, Newcastle University, Newcastle upon Tyne NE1 7RU, United Kingdom

ARTICLE INFO

Editor: Claudia Romano

Keywords:
Hydraulic fracturing
Flowback and produced water
Environmental geochemistry

ABSTRACT

The combination of hydraulic fracturing with horizontal drilling has revolutionized oil and gas production. However, most of our understanding of the subsurface mechanisms and chemical interactions that occur during the process come from analyses of flowback and produced water (FPW). While the chemical composition of FPW can provide some information to understand water-rock interactions in the subsurface, the mechanisms by which dissolved species, including potentially toxic heavy metals (PTHM), are mobilized remain poorly constrained. In this study, we used stirred benchtop reactors to simulate the geochemical processes that occur when injected hydraulic fracturing fluid (HFF) interacts with reservoir rock formations of the Upper Devonian Duvernay Formation, a mudstone formation that is an important hydraulic fracturing target in west-central Alberta, Canada. Our aims were to: (1) assess whether our laboratory methods can be used to predict the inorganic chemistry of FPW, including concentrations of PTHM, and (2) to ascertain the reaction kinetics and mechanisms of the release of inorganic components from reservoir rocks. Our results indicate that elemental concentration data from reactor experiments coupled with saturation indices modelling can be used to predict the assemblage of solid phases that precipitates downhole, such as barite + celestine + gypsum. High salinity experiments (0.5 M NaCl), simulating FPW reuse, showed increased concentrations of many dissolved species with increasing salinity. Our findings were corroborated with geochemical modelling of FPW samples collected from operating unconventional wells in the Duvernay Formation. FPW from wells using a mixture of recycled produced water (RPW) and fresh source water to make up the injected HFF had higher concentrations of many elements, including the PTHM, Ba, Sr, and As. Our work illustrates the potential environmental risks of using RPW in hydraulic fracturing operations in the event of a spill and it provides a robust benchtop approach to predict the leaching of elements from the host rock during hydraulic fracturing.

1. Introduction

Hydraulic fracturing combined with horizontal drilling is used for the recovery of oil and gas from low-permeability unconventional reservoirs where conventional oil and gas recovery would otherwise be uneconomic. Hydraulic fracturing requires considerable quantities of water, with the median volume varying between 15,275 m^3 and 19,425 m^3 in the United States (Gallegos et al., 2015). The quantity of water used in hydraulic fracturing is expected to rise with the drilling of longer horizontal wells (Gallegos et al., 2015; Alessi et al., 2017). Most commonly, water is acquired from nearby surface water or shallow groundwater, with brackish groundwater used less frequently (Goss et al., 2015). The water is mixed with chemical additives to make up hydraulic fracturing fluid (HFF) before being injected to fracture the reservoir rock. The composition of HFF varies based on mineralogy of the target formation. Typically, the mixture is predominately water, with chemical additives only contributing a small percentage (<1%) of the bulk composition by volume (Arthur et al., 2008; Alessi et al., 2017). Following fracturing, when FPW returns from the well, it has variable total dissolved solids (TDS) content depending on the mineralogical composition of the formation, the scale of the induced fracturing and the amount of time after flowback began. For example, FPW from the

* Corresponding author.
E-mail address: snihur@ualberta.ca (K.N. Snihur).

https://doi.org/10.1016/j.chemgeo.2022.120718
Received 10 September 2021; Received in revised form 29 December 2021; Accepted 4 January 2022
Available online 6 January 2022

Marcellus Formation shales in the Eastern USA ranges between 8000 ppm – 360,000 ppm TDS (Shaffer et al., 2013; Abualfaraj et al., 2014), whereas FPW from the Duvernay Formation in Western Canada varies from less than 10,000 ppm in early flowback (i.e., in the first 24 h) to greater than 200,000 ppm in produced waters (usually ~2 weeks after initial flowback) (Alessi et al., 2017; He et al., 2017; Zhong et al., 2019). The TDS is mostly composed of salts either from formation brines or leached from the fractured formation (Ziemkiewicz and He, 2015). In addition to dissolved salts, FPW also contains potentially toxic heavy metals (PTHM), as well as organic compounds (e.g., polyaromatic hydrocarbons; PAHs), residual HFF additives and their transformation products, and other hydrocarbon range organic compounds (He et al., 2017; Flynn et al., 2019).

In some cases, HFF is made using a mixture of freshwater and FPW from previous fracturing operations (Zhong et al., 2019). FPW that has been recycled to make HFF for another well is often referred to as recycled produced water (RPW). In Alberta, the targeted salinity for RPW is approximately that of seawater or 30,000 ppm in total dissolved solids (TDS) (Sun et al., 2019). While RPW was only used in 2% of hydraulically fractured wells in Alberta in 2018 (AER, 2019), the practice is increasing in areas of the United States, with 25% of water used in hydraulic fracturing in the Marcellus Formation being sourced from recycled produced waters as of 2014 (Shaffer et al., 2013; Barth-Naftilan et al., 2015). Using RPW instead of freshwater is viewed as a more environmentally friendly practice, as it reduces use of additional freshwater resources, such as shallow groundwater, lakes, and rivers, which are suitable for agricultural and drinking water (CAPP, 2018). It also reduces the need for FPW disposal via deep well injection.

Recent studies have focused on the factors that determine FPW geochemistry by describing water-rock interactions between HFF, formation water, and the target formation (Tasker et al., 2016; Harrison et al., 2017; Sumner and Plata, 2018; Xiong et al., 2018; Flynn et al., 2019; Li et al., 2019; Li et al., 2020; Owen et al., 2020). While some studies focused solely on FPW chemistry (e.g., Flynn et al., 2019; Owen et al., 2020), there have also been attempts to experimentally replicate the formation temperatures and/or pressures achieved during hydraulic fracturing (Tasker et al., 2016; Harrison et al., 2017; Sumner and Plata, 2018; Xiong et al., 2018; Li et al., 2019; Li et al., 2020). For example, in the Duvernay Formation the temperature is approximately 115 °C (Taylor et al., 2014) and the pressure is between 600 and 850 bar (Shen et al., 2018); however, both temperature and pressure will vary between formations and even within a formation.

FPW typically contains elements not used in hydraulic fracturing additives or found in abundance in fresh source waters, such as PTHM (e.g., Ba, Sr, and As). The consensus is that the main sources of dissolved constituents in FPW are either leached from the formation or via mixing with formation waters (Rowan et al., 2015; Owen et al., 2020). While leaching from the formation and interactions with formation waters are likely the dominant drivers of the composition of FPW, the relative contribution of each process to the final FPW chemistry is not well constrained. Inverse modelling using inorganic elemental concentrations in HFF and FPW has been employed to explain the interactions between HFF, formation water and rock (Owen et al., 2020), but the results have yet to be verified experimentally. Recent work using benchtop reactors has begun to elucidate the organic and inorganic geochemical interactions that occur during hydraulic fracturing (Tasker et al., 2016; Harrison et al., 2017; Sumner and Plata, 2018; Xiong et al., 2018; Li et al., 2019; Li et al., 2020; Hakala et al., 2021). These studies show that the temperature of reaction, pH and ionic strength of the simulated HFF impact the mobilization of PTHM and degradation of organics, while pressure had a limited effect. Although the leaching of elements from shale at elevated pressures and temperatures has been studied extensively, the relationship between geochemical results obtained from laboratory reactors and those measured directly using FPW from hydraulically fractured wells has not been described in detail. Accordingly, we tested whether simple, low-cost, benchtop reactors containing mixtures of water and target rock particles at reservoir temperatures could be used to predict the measured inorganic chemistry profile of FPW. Specifically, we aimed to; (1) constrain how the salinity of RPW impacts metals leaching from formation rocks during the hydraulic fracturing process, and (2) assess whether the reactors and methods developed here can be used to predict and address the problem of scaling.

2. Materials and methods

2.1. Formation of study

Rock samples were collected from outcrop samples of the Perdrix Formation, while cores were collected from the Duvernay Formation (Fig. S1). FPW samples were collected from hydraulically fractured wells in the Duvernay Formation of west-central Alberta (Well IDs: 103/01–12-063-21 W5 and 100/12–30-063-21 W5; Fig. 1). Additional information about rock and FPW sampling and locations is provided in the supplementary information. Time-dependent geochemical data for the FPW from these wells are published in Zhong et al. (2019).

2.2. Experimental design

Outcrop and core samples were ground and sieved to between 0.09 mm and 0.5 mm to ensure the particles would pass through the needle (18G or 1 mm) used for sampling during the experiments. Experiments were conducted in reactor vessels at 25 °C, 95 °C, and 140 °C (supplementary information). Reactor experiments using the outcrop samples were used to assess the kinetics of leaching and the mobilization of ions at all three temperatures, 25 °C, 95 °C, and 140 °C, prior to similar experiments using limited core samples, conducted at the temperature of the formations. Experiments with core materials from the Duvernay Formation were conducted at the corresponding reservoir temperatures for each core: 95 °C and 140 °C for Cores 1 and 2, respectively (calculations provided in supplemental information). An initial water-rock ratio of 18:1 was used for all experiments to prevent clogging during sampling. The exact volumes, masses and temperatures are provided in Table S1. Reactor experiments were conducted with both ultrapure water (18.2 MΩ·cm) and a solution of 0.5 M NaCl. They were then allowed to reach a natural pH (pH values are reported in Table S7) to simulate the interactions between the rock and HFF made from either freshwater, or a mixture of freshwater and recycled produced water or brackish-saline groundwater, and were subsequently compared with FPW from corresponding wells. All experiments conducted with the core samples were done in duplicate for both type A and B reactors (described in detail in the supplemental information; Fig. S2). Experiments were allowed to run for 48–168 h depending on the experiment type, and were sampled at regular intervals (Table S2). Following sampling, the slurry aliquots were filtered using 0.8 μm cellulose acetate membranes. The solids retained on the filters were dried and weighed to account for the mass change within the reactor. The mass and pH of the filtrate were recorded before it was separated into two vials, one unacidified and one acidified with 12 μL 70% nitric acid per 10 mL of sample. Samples were then refrigerated until analysis.

2.3. Aqueous analyses

2.3.1. Elemental analyses

Filtrates were analysed for major and trace elements using an Agilent 8800 inductively coupled plasma mass spectrometer (ICP-MS/MS) at the University of Alberta. Where required, dilutions were done with 18.2 MΩ·cm ultrapure water and samples were re-acidified with 12 μL of 70% HNO_3 per 10 mL solution prior to analysis. During analysis, no-gas mode was used for low mass elements and heavy metals, while a gas collision/reaction cell was utilized for most of the elements — either He, O_2, or H_2 depending on the element, with all methods using tandem MS/MS mode

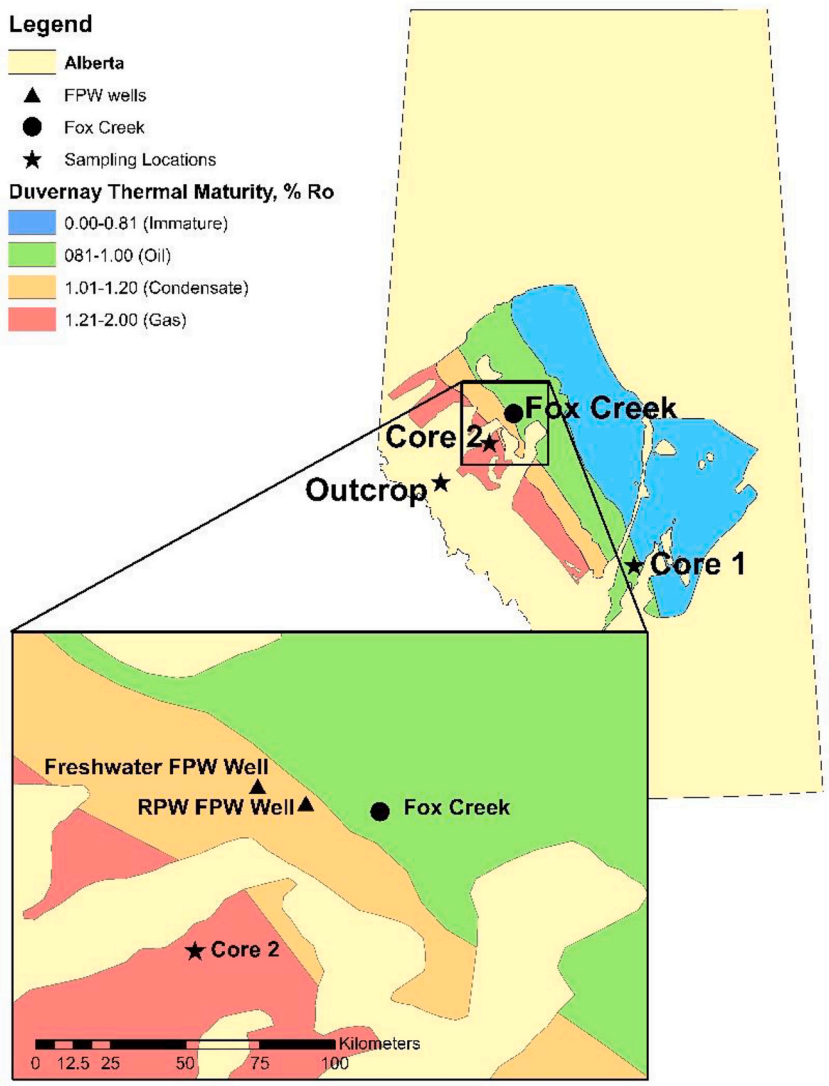

Fig. 1. Map the Duvernay Formation with the locations of the wells from which FPW samples were collected with respect to Core 1, Core 2, and the Outcrop samples. Thermal maturity boundaries derived from Hackley and Cardott (2016).

(Table S3). An internal standard mix containing Sc, Ge, In, Lu, and Bi was introduced using an inline addition to account for instrumental drift. For Core 1 experiments, Cl concentrations were measured with colorimetry using EPA method 325.2. For this method, ferricyanide forms a colored complex with Cl^-, which was measured with a Thermo Gallery Plus Beermaster Autoanalyzer. For Core 2 and the outcrop experiments, Cl was measured with ICP-MS/MS.

2.3.2. Alkalinity measurements

Alkalinity was measured for aqueous samples derived from reactor experiments with Core 2 and the outcrop rocks, using the unacidified portion of the filtrate following the method outlined in Flynn et al. (2019). For each measurement, a 5–7 mL volume of filtrate was titrated with 0.1 M HCl to a pH of 4.2 using a Metrohm Titrando 905. The milliequivalents of acid used to lower the pH were used to calculate the alkalinity. These analyses revealed a relatively constant ratio of 7:5 for $Ca:CO_3$, the ratio was used to calculate alkalinity for Core 1 reactor experiments to ensure solution mass balances and allow for geochemical modelling due to sample volume limitations.

2.4. Solids analysis

2.4.1. Total acid digestions

A total acid digestion of each solid sample was conducted based on the method outlined in Wang et al. (2016). The method was modified to include the addition of 20 mL boric acid to prevent the formation of insoluble fluoride precipitates (Wilson et al., 2006). One in every 10 samples was digested in duplicate for error analysis. Boquillas Shale, ShBOQ-1 (Birdwell, 2017), was used as a standard reference material to quantify methodological error. The digestate elemental composition was determined using an ICP-MS/MS following a method similar to that used to analyze aqueous samples. A complete list of ICP-MS/MS parameters and metals measured for the digested solids is listed in Table S4.

2.4.2. Powder X-ray diffraction (XRD)

Samples with a total mass $\geq$ 1 g were ground under anhydrous ethanol using agate elements with a McCrone Micronizing Mill for 7 min. Samples with masses between 0.5 g and 1 g were milled for 5 min using a miniaturized McCrone grinding vessel (using the design of Locock et al., 2012). All samples were dried at room temperature overnight, and disaggregated using an agate mortar and pestle.

Samples were prepared in front-loading cavity mounts for analysis.

Patterns were collected using a Bruker D8 Advance powder X-ray diffractometer equipped with LYNXEYE XE-T linear position sensitive detector and a cobalt source that was operated at 35 kV and 40 mA. XRD patterns were collected from 3°–80° 2θ using a step size of 0.02° 2θ and a dwell time of 1 s/step. Mineral phase identification was conducted using the DIFFRAC.EVA XRD phase analysis software (Bruker) with reference to the International Center for Diffraction Data Powder Diffraction File 4+ database (ICDD PDF4+). Rietveld refinement (Rietveld, 1969; Hill and Howard, 1987; Bish and Howard, 1988) with XRD data was utilized to determine mineral abundances with TOPAS 5 (Bruker). Fundamental parameters peak fitting (Cheary and Coelho, 1992) was used for all phases including the clay minerals.

2.4.3. TOC/TIC

Total organic carbon (TOC) and total inorganic carbon (TIC) were measured using a Leco RC612 Carbon Analyzer. Each sample was loaded into the furnace in a quartz boat that was previously cleaned via heating for 5 min in a 1000 °C furnace. During each run, the furnace temperature was increased from 100 °C to 1000 °C over 15 min and the CO_2 generated was measured as a function of time using an infrared sensor. CO_2 generated with corresponding H_2O was used to quantify TOC and the total CO_2 over the temperature ramp was used to quantify the TC. The total inorganic carbon content was calculated by the difference between the TC and TOC.

2.5. Saturation indices modelling

Chemical speciation modelling for saturation indices was conducted using PHREEQC v. 3.5 (Parkhurst and Appelo, 2013). The pitzer.dat database was used for high ionic strength experiments (0.5 M), while the phreeqc.dat database was used for the experiments conducted at lower ionic strengths (<0.1 M). Saturation indices were calculated using aqueous elemental concentrations in an approach similar to that used by Flynn et al. (2019). Briefly, saturation indices of amorphous silica ($SiO_{2(am)}$), quartz (SiO_2), calcite ($CaCO_3$) barite ($BaSO_4$), celestine ($SrSO_4$), anhydrite ($CaSO_4$) and gypsum ($CaSO_4{\cdot}2H_2O$) were calculated at each sampling point for the duration of each experiment. These phases were selected because they were either measured in abundance in the original source rock, or they are typical minerals that precipitate during hydraulic fracturing (Flynn et al., 2019). All major elements (>0.5 mmol/L) and important trace elements, such as Ba and Sr, there were available in both databases (pitzer.dat and phreeqc.dat) were used in modelling calculations. Hörbrand et al. (2018), studying the performance of common databases used in PHREEQC at extreme conditions, showed that the Pitzer database most closely resembles the results of the phreeqc.dat database, used for the freshwater experiments, supporting our database selections.

3. Results

3.1. Mineralogy and lithogeochemistry

Core 1 from the Eastern Shale Basin had a higher proportion of calcite (61.2 wt% by mass) versus Core 2 from the Western Shale Basin (56.0 wt%). However, the total carbonate mineral content was comparable within typical values for refinement error in our laboratory (66.2 wt% in Core 1 and 68.5 wt% in Core 2) (Fig. 2). By comparison, the outcrop sample was dominated by quartz (52.4 wt% in the outcrop versus vs 7.3 wt% and 19.6 wt% for Core 1 and Core 2, respectively) with carbonate minerals only comprising 15.9 wt%. Core 1 was found to have the highest and most diverse clay mineral content, with illite, clinochlore (Mg-rich chlorite) and kaolinite collectively making up a total 13.3 wt% of the total rock composition, while illite was the only clay mineral found in the outcrop (11.9 wt%) and Core 2 (3.7 wt%) samples. Gypsum, a common product of pyrite oxidation and calcite dissolution, was the only mineral found exclusively in the outcrop samples.

Consistent with the mineralogical data, Ca and Mg were the dominant cations in the core samples, comprising 48.8 wt% and 55.8 wt% of the overall measured composition in Core 1 and Core 2, respectively. Silicon, associated with quartz and other silicate minerals, made up 30 wt% of the measured composition of the cores. The remainder of the major cations are commonly found in silicate minerals (e.g., Na, Al, and

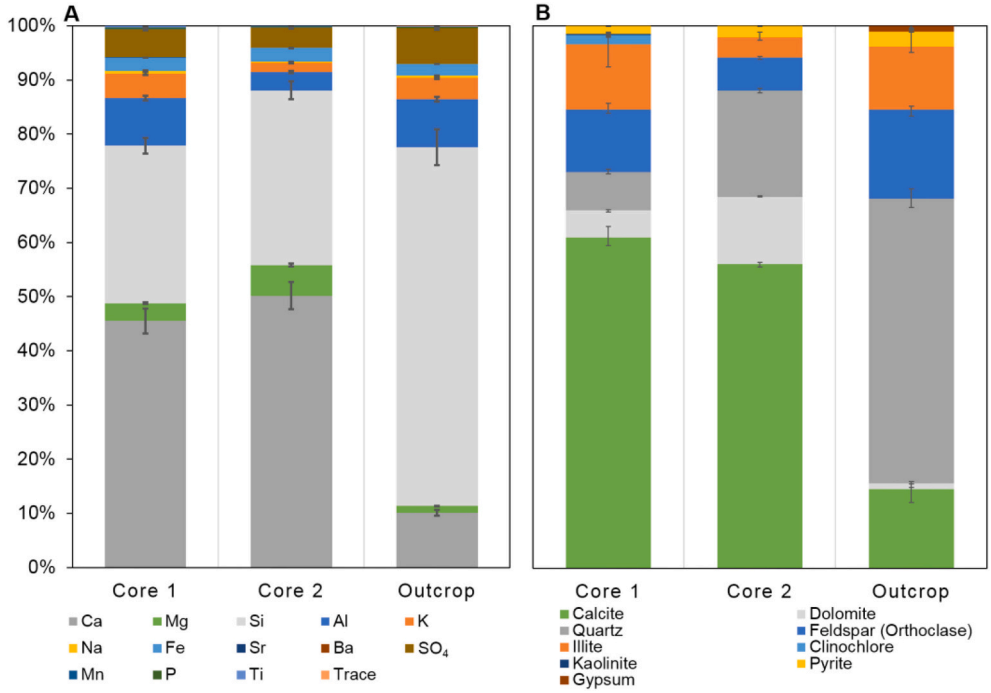

Fig. 2. Average compositions of rock samples used in experiments. The major cations and anions (>1 wt%) and mineral abundances are presented in (A) and (B), respectively. Major elements represent >99.9 wt% of the total measured composition of the rock samples (excludes O and C), while the trace metals are defined as making up less than 0.1 wt% of the rock composition. Error bars represent ±1σ.

K), sulfide/sulfate minerals (e.g., Fe, Sr, and Ba), and accessory oxides that were present below the detection limits of our XRD analysis (e.g., Ti and Mn). The mineralogical differences between the core samples and the outcrop were reflected in the elemental composition, with a 3-fold higher concentration of Si in the quartz-rich outcrop samples compared to the core samples. The major elements identified using total acid digestion made up 99.9 wt% or more of the measured rock composition (excluding O and C), with trace elements making up the remaining 0.1 wt% or less. The similarity in trace element concentrations amongst the core samples, coupled with the comparable abundance of pyrite in the core samples and outcrop samples, allowed for the more abundant outcrop samples to be used for method development and temperature dependence experiments, in lieu of the scarcer core samples.

The mineralogical compositions of outcrop and core samples showed minimal change during the leaching experiments (Table S5). No new phases were detected in the experiments, and only small changes were observed in both the core and the outcrop experiments. Because the changes were minor, and consistent with sample heterogeneity and typical refinement errors, the changes in the bulk mineralogy of the core samples were assumed to be negligible throughout the duration of the experiments. The mineralogical changes in the outcrop sample were also minimal; except for the complete loss of the accessory mineral, gypsum (Table S5).

The total digestion data gave a better understanding of which elements were leached from the outcrop and core samples and the reactions that occurred during the experiments. The elemental concentrations show minor decreases in abundances of the elements measured (Table S6). The only element to show a substantial decrease in the rock samples was Mo, with up to 11% of total Mo leached from Core 1 material in the 0.5 M NaCl experiments. For comparison, less than 0.1% of most other transition metals were leached from outcrop and core samples during the experiments (Table S6). Total carbon fractions remained constant throughout the experiments, with preferential release of inorganic carbon relative to organic carbon (Fig. S3).

3.2. Aqueous chemistry of experiments

Aqueous geochemistry profiles were constructed to illustrate the trends of elements associated with the most abundant primary minerals, e.g., quartz, calcite, and gypsum, and common accessory minerals found in the solid fraction of FPW, e.g., barite and celestine. This includes Ca, Si, SO_4, Sr, and Ba (Fig. 3). Additional elemental concentration profiles are plotted in Fig. S4. In most of the experiments, major elements such as Ca, Si, and SO_4, and Mg (Fig. S4) showed an increased leaching, or salting-in effect, in the 0.5 M NaCl experiments due to the higher ionic strength. This was not the case for Ca and SO_4 with Core 1 experiments (Fig. 3a,g) and the 95 °C outcrop experiments (Fig. 3c,i), which either had no difference in leaching or a salting-out effect, with the freshwater experiments leaching more Ca and SO_4 than the higher ionic strength NaCl experiments. Aqueous species typically derived from the weathering of evaporite minerals such as halite or gypsum (Na, Cl, Ca, and

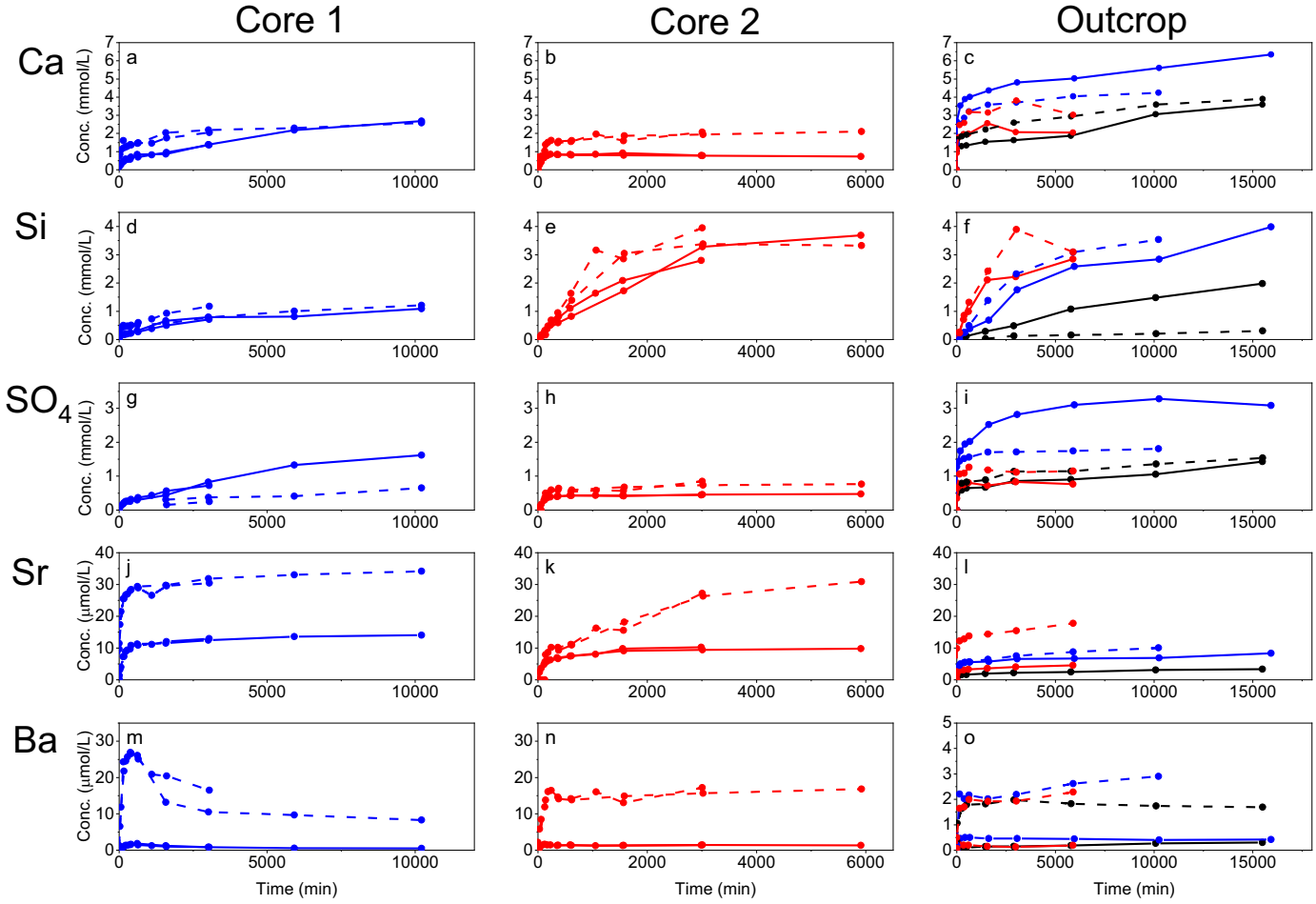

Fig. 3. Aqueous geochemical profiles for Ca (a-c), Si (d-f), SO_4 (g-i), Sr (j-l), and Ba (m-o) of Core 1 (a, d, g, j, m), Core 2 (b, e, h, k, n), and Outcrop (c, f, I, l, o). Experiments were conducted at 25 °C (black), 95 °C (blue), and 140 °C (red), 0.5 M NaCl experiments are represented by dashed lines and freshwater with solid lines. Errors are reported in Table S7 and represent ±1σ, $n = 3$. (For interpretation of the references to colour in this figure legend, the reader is referred to the web version of this article.)

SO_4) or carbonate minerals (Ca, Mg, CO_3), on average reached equilibrium sooner than those typically found in silicates (Si, K) (Fig. 3; Table S7). Some trace elements, such as Ba and Sr, also reached equilibrium early in the experiments, with Ba reaching equilibrium sooner than Sr, likely owing to its decreased solubility in barite when compared to Sr in celestine.

Due to the initially oxic conditions of the reactor experiments, the total sulfur determined using ICP-MS/MS was assumed to represent the concentration of dissolved sulfate. This assumption is supported by Fe (II) not being detected in measurable amounts in the aqueous phase despite its considerable concentration in the host rocks. If present, Fe(II) would oxidize and rapidly precipitate at the experimental pH levels (6–8), as a ferric oxyhydroxide, such as ferrihydrite (approximately $Fe(OH)_{3(s)}$), in contrast to reducing experimental conditions where iron would remain in solution as $Fe^{2+}_{(aq)}$ (Jew et al., 2017; Li et al., 2019). Core 1 (Fig. 3g) had 2.5× more sulfate leached in the freshwater experiments compared to the NaCl experiments likely due to a lag in the kinetics because of the hydration of Na^+ and Cl^- ions by water (Azimi, 2010) at that temperature (95 °C). In the outcrop experiments, this salting-out effect was also observed and is consistent with the dissolution of gypsum, which has its peak solubility between 50 °C and 100 °C, as there was nearly 4× as much gypsum (2.2 wt% versus 0.5–0.9 wt%) in the input rock for the freshwater experiment at 95 °C than in the 0.5 M NaCl experiment (Table S5). As the aqueous data indicate that ~2.5% of the gypsum was dissolved, either gypsum did not fully dissolve, and/or there was subsequent precipitation of minerals bearing Ca and SO_4 that were not detected with XRD. The lack of evidence for the precipitation of Ca- and SO_4-bearing minerals may indicate that they are associated with several trace minerals, such as barite, or celestine that were below the detection limit of XRD or are present as a poorly ordered solid phase. Core 2 at 140 °C, on the other hand, had an initial increase in SO_4 concentration over the first 2–4 h, reaching a plateau at 0.4 mmol/L and 0.7 mmol/L in the freshwater and NaCl experiments, respectively, by the end of the experiment. This indicates a distinct salting-in effect of approximately 1.75× in the 0.5 M NaCl experiments. The peak solubility of sulfate-bearing minerals, such as gypsum and kieserite ($MgSO_4{\cdot}H_2O$), is typically between 25 °C and 95 °C, with a decline in solubility at temperatures greater than 100 °C; this is a common trait amongst sulfate minerals (e.g., Rosenbauer et al., 2005; Krumgalz, 2018). The sulfate trends seen in the 140 °C experiments of both Core 2 and the outcrop sample mirror those of Mg (Fig. S4b,c), suggesting that a Mg-sulfate mineral, such as epsomite ($MgSO_4{\cdot}7H_2O$), could have been present in concentrations below the detection limit of XRD.

The last major ion of interest, Si, was found not to reach equilibrium with mineral phases during the experimental time frames for outcrop and core samples in all experiments (Fig. 3d-f). This was consistent with previous reactor experiments conducted by Harrison et al. (2017) which found that Si remained undersaturated with respect to quartz even after 500 h (~21 days) (Morey et al., 1962). The increased leaching of Si observed in the Core 2 experiments relative to Core 1 was due to the increased temperature of those experiments (140 °C versus 95 °C), which either accelerated the kinetics, or increased the solubility of quartz and other silicate minerals (Siever, 1962). While the aqueous concentration of silica did not approach equilibrium with quartz, there was substantial leaching of Si from the rock (10% and 41% relative of the total leached ions for Core 1 and Core 2, respectively). Ionic strength had no discernible effect on the dissolution of silicate minerals in either the Core 1 or Core 2 experiments. It did, however, have a small impact on silicate mineral dissolution in the outcrop experiments, although equilibrium was not reached.

The concentration profiles of Sr and Ba, as well as As, were investigated due to their potential to form mineral scales in infrastructure and/or their toxicity, respectively (Fig. 3j-o, Fig. S4j-l). Both core samples leached similar Sr concentrations at steady state, equilibrating at 10 μmol/L and 30 μmol/L in freshwater and NaCl experiments, respectively, while the outcrop experiments had slightly lower concentrations (equilibrating at Sr concentrations of 2–18 μmol/L depending on the experimental conditions). Additionally, the concentration of Sr increased with ionic strength, with a 3-fold greater release of Sr in the 0.5 M NaCl experiments with the cores and a 2- to 4-fold release of Sr in the outcrop experiments. In the freshwater experiments, there was an initial increase in Sr concentration to 8.5 μmol/L over the first 2 h which subsequently plateaued between 10 and 15 μmol/L after 24 h for both core samples. By contrast, for the saline experiments the aqueous Sr concentrations in experiments using Core 1 plateaued at 30 μmol/L after 24 h while those for Core 2 increased more slowly, reaching the same concentration only after 96 h without plateauing over the duration of the experiments. The concentration of Sr leached from the rock samples appeared to be influenced by both temperature and the ionic strength of the experimental solution, with increased leaching observed when either temperature or ionic strength were increased. No Sr was detected in solution during the 25 °C NaCl experiment using outcrop material, likely due to the higher dilution required for analysis (Fig. 3l).

Low concentrations of Ba were leached into solution in all experiments (<30 μmol/L), (Fig. 3m-o). Similar to what was observed for Sr, a strong salting-in effect was observed for Ba in the 0.5 M NaCl experiments of 17×, 12×, and 9–10× compared to the freshwater experiments for Core 1, Core 2, and the outcrop sample, respectively, after 96 h. The freshwater experiments for both cores showed an early peak in Ba concentration in solution at the time the reactor reached the target temperature, 95 °C for Core 1 and 140 °C for Core 2 (1.8 μmol/L and 1.6 μmol/L, respectively). This was also observed in the outcrop experiments with freshwater at all three temperatures. The initial peaks in Ba concentrations were followed by a stabilization at lower concentrations for all rock types. This trend was also observed in the saline experiments using Core 1 but in a more pronounced manner (Fig. 3n), with a higher peak concentration of 27 μmol/L. This transient peak in the concentration of aqueous Ba, at T_0 of the experiment, is approximately 2.5× higher than the final concentrations measured after 1 week. In saline experiments using Core 2 and the outcrop experiments, this trend was not observed. Unlike Sr, the concentration of Ba was not significantly affected by temperature, but did show changes in concentration due to ionic strength (Fig. 3o).

The concentration profile of As, which is important in FPW due to its potentially toxic effect on aquatic life at low concentrations (e.g., Delompré et al., 2019; Folkerts et al., 2020; Mehler et al., 2020), can be found in Fig. S4 along with Al, K, and Mo. Because the detected concentrations of As were near the detection limit of our analysis, the trends observed between the freshwater and 0.5 M NaCl experiments were less than the error in quantification, and therefore not statistically significant. Additional anion concentration profiles can be found in Fig. S5.

4. Discussion

4.1. Comparison of fluids from reactor experiments with FPW

The results from the reactor leaching experiments were compared to the FPW from two hydraulically fractured wells from the Duvernay Formation, one that used recycled produced water (RPW) to make up the injected HFF, while the other exclusively used freshwater. The FPW from these wells will be referred to as RPW FPW and freshwater FPW, respectively. Both wells are located in the West Shale Basin of the Duvernay Formation, approximately 55 km from the borehole where Core 2 was obtained, near Fox Creek, AB (Fig. 1). The wells are not of equal thermal maturity either both core, but fall in between the thermal maturities of Core 1 and 2.

4.1.1. Chemical data

Both FPW samples had higher aqueous concentrations of all measured elements than the reactor experiments. While absolute concentrations and some order of relative abundances vary slightly between the FPW and the leaching experiments, the grouping of major (B, Ca, K,

Mg, Na, and Sr) and minor/trace cations (Al, As, Ba, Fe, Mn, Mo, Ti, Zn) were identical except for Si. The latter was not present at concentrations above the detection limit in FPW samples from either well taken at 48 h after initial flowback but was detected in both freshwater and NaCl experiments conducted in the laboratory (1–3 mmol/L). This general consistency in elemental abundances in reactor fluids with those of FPW supports our contention that the methodology used in our experiments replicated the major water-rock interactions that occur during hydraulic fracturing. The observed differences, particularly in absolute ion concentrations, are at least in part due to differing water-rock ratios between those used when fracturing the wells and that used in our experiments, but the results indicate that the metals found in FPW are primarily sourced from the leaching and dissolution of minerals in the host rock during hydraulic fracturing. For example, Ca and Mg, which were amongst the highest concentration elements dissolved in our reactor experiments (1–5 mmol/L and 0.1–1 mmol/L, for Ca and Mg, respectively), were likely sourced from the dissolution of the carbonate minerals, e.g., calcite and dolomite [$CaMg(CO_3)_2$]. Additionally, the dissolution or desorption of ions from some silicate minerals, such as K-feldspars ($KAlSi_3O_8$), quartz, and clay minerals, such as clinochlore [$(Mg,Fe^{++})_5Al(Si_3Al)O_{10}(OH)_8$], illite {$(K,H_3O)(Al,Mg,Fe)_2(Si,Al)_4O_{10}[(OH)_2,(H_2O)]$}, and kaolinite ($Al_2Si_2O_5(OH)_4$), can introduce elements, such as Si, Na, K, and Al, into solution all. Indeed, these were measured in high concentrations relative to other measured elements in our experimental solutions (Tables S8 and S9).

There are two main theories for the primary TDS source in FPW: (1) formation water or (2) leaching that occurs as a result of HFF interactions with reservoir rock (Rowan et al., 2015; Owen et al., 2020). The bulk of FPW TDS (> 90%) is composed of Na and Cl, regardless of the mixing water used to make the HFF (Tables S8 and S9). As a fraction of the total elemental composition, the freshwater reactor experiments (with no added NaCl) had considerably less Na and Cl than either FPW sample. This indicates that most of the Na and Cl in the FPW likely originated from pore brines that were released during fracturing. Those brines were not present in measurable quantities in the core samples and were likely heterogeneously distributed in host rock fractures. These isolated fractures may have arisen from the fracturing process itself, but are unlikely to be present in the cm-scale core samples used for these experiments.

The formation water is not believed to be a significant source of aqueous Fe(II). Although pyrite was identified in all the rock samples used in our experiments at several wt% abundance, and it is reasonable to interpret that it was the primary source of Fe in the experiments, no Fe (II) was detected in solution. Recent work by Jew et al. (2017) and Li et al. (2019) found that aqueous Fe(II) concentrations in simulated hydraulic fracturing experiments were controlled by the pH of the experimental solutions. Lower pH values (pH of ~2) slowed the oxidation of leached Fe(II) and formation of relatively insoluble ferric oxyhydroxide minerals. Our experimental solutions were consistently between pH 6 and 8 and any leached Fe(II) would have likely oxidized rapidly to form a precipitate. While no ferric oxyhydroxide minerals were identified in the rock samples following the experiments, it is well known that those minerals are difficult to detect using diffraction techniques owing to their nanocrystalline or amorphous nature. Flynn et al. (2019) also identified amorphous ferric oxyhydroxide in the solid fraction of FPW that was undetectable by XRD.

The relative abundances of five selected major elements (Mg, Ca, Si, K, and S) from both the FPW samples (after 48 h of FPW flow) and our experiments (48 h after the target temperature was reached) were compared (Fig. 4). There was a substantially greater fraction of dissolved Ca in the FPW samples (68–70% of the total measured composition of FPW vs 12–24% in reactor experiments, after the exclusion of

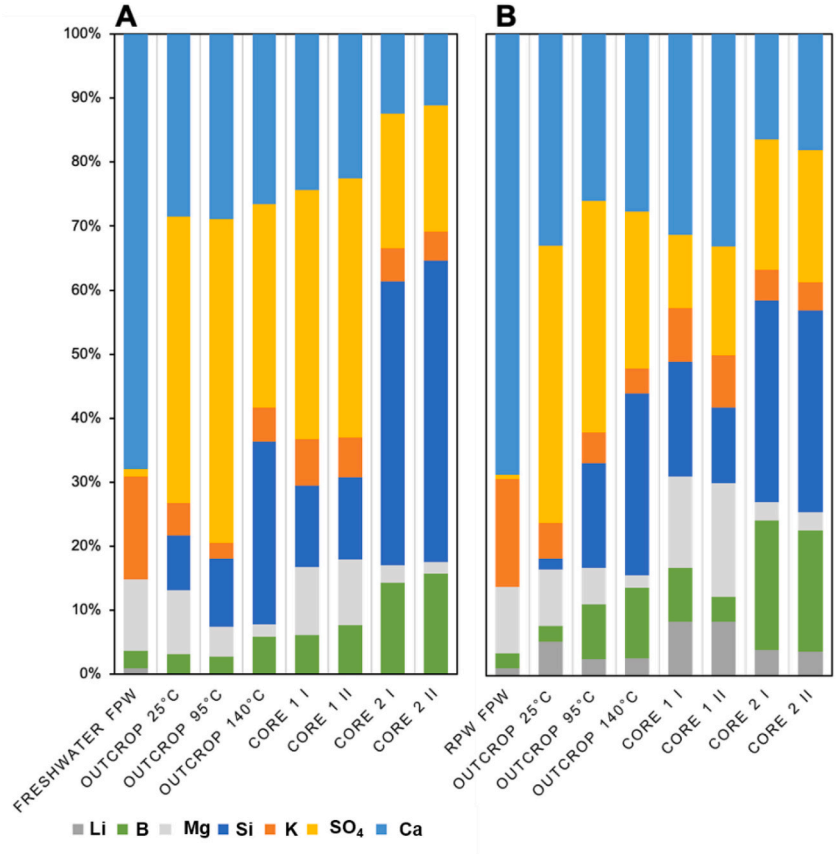

Fig. 4. Element distribution of major ions in solution (>1% relative) with the exclusion of Na and Cl. (A) Freshwater FPW was compared with pure water reactor experiments (B) and RPW FPW were compared with 0.5 M NaCl reactor experiments.

Na and Cl), owing to its presence in formation water or increased dissolution from the formation because of the low initial pH of HFF due to the addition of acids. As K is also a common component of HFF additives, its higher relative abundance in the FPW samples can possibly be accounted for, although the composition of the additives was proprietary information and not disclosed. In a recent study, Owen et al. (2020) found that SO_4 in solution was best modelled as being derived from the dissolution of pyrite and subsequent oxidation, and is probably the mechanism by which sulfur was entering into solution in both the FPW and our reactor experiments. Li et al. (2019) also found that pyrite oxidation was a significant source of sulfate during reactor experiments of similar design to those in this study. Despite this and the far higher water-rock ratio in our reactor experiments, SO_4 concentrations in reactor experiments were comparable to those measured in FPW: 1–5 mmol/L (Tables S8 and S9). Although barite was not detected at any point during the experiments with XRD, trace amounts were likely precipitating out and buffering the aqueous sulfate concentrations, as the solution was in equilibrium with barite for the duration of the experiments. As the TDS of the reactor experiments was far lower than that of FPW, the relative fraction of SO_4 in those experiments was far greater: 18–50% in freshwater experiments and between 0.07 and 0.58% in 0.5 M NaCl experiments. Given that the absolute concentrations of SO_4 in the reactor experiments were consistent with those measured in both FPW samples, it is probable that the aqueous concentrations of sulfate are being controlled by barite precipitation, which has a low solubility, and drives additional dissolution of sulfur bearing minerals, such as pyrite.

4.1.2. Saturation indices

In all three rock samples, quartz and calcite were found to be the dominant minerals comprising greater than 67 wt% of each sample. These two minerals are likely to control the aqueous concentrations of Si and Ca, and therefore, both were used to compare FPW solution chemistry with the saturation index (SI) approach. The SI for calcite and quartz were calculated from the aqueous concentrations of ions measured during the reactor experiments and from the aqueous geochemistry of FPW. Despite the chemical profiles of Si and Ca not reaching steady state during the experimental timeframe (Fig. 4) in both core samples and outcrop samples experiments, the calculated SI values of quartz and calcite were at, or near, equilibrium (Fig. 5). Amorphous silica, the amorphous counterpart to quartz, was also included in the models, but the solutions consistently remained undersaturated with respect to this phase, indicating the solutions were in equilibrium with quartz and not amorphous silica (Fig. S6a-d). As the freshwater FPW component concentrations reported in Zhong et al. (2019) did not include DIC concentrations, the SI for calcite was not determined for that sample (Fig. 5d). Additionally, aqueous Si was below the detection limit at all time points for both sets of field-collected FPW samples, with the exception of the final time point from the freshwater FPW (T_{225hr}), due to the higher dilution required for analysis (Fig. 5h).

The calcite SI for both cores showed an initial dip in magnitude to less than 0, followed by a return to near equilibrium conditions, with SI values ending at, or near, equilibrium regardless of the ionic strength of the solution (Fig. 5a,b). In outcrop experiments using RPW FPW, equilibrium was not reached between the solution and calcite regardless of temperature or ionic strength (Fig. 5c,d). In general, the calcite SI value modelled for the RPW FPW was lower than those for the reactor experiments, with the exception of the 25 °C reactor experiments with the outcrop sample. This likely indicates that formation water contributes to the composition of the RPW FPW or that the DIC content of RPW FPW degassed before it could be measured at the surface following collection. As this effect was only observed for the DIC and the Ca concentrations are comparable to it, degassing is the most probable cause of the disparity. Coincidentally, the DIC concentrations from the outcrop experiments were comparable to that of the RPW FPW, despite their differences in TDS. DIC makes up a much smaller fraction of the FPW (Zhong et al., 2019; Tables S8 and S9), and hence limits the precipitation of calcite and other carbonate minerals. This finding suggests that the DIC content of FPW is almost entirely due to leaching from the formation or interactions with the atmosphere and not from the HFF. Indeed, the DIC is most probably from the dissolution of carbonate minerals in the formation similar to the findings of previous studies (Paukert Vankeuren et al., 2017). Moreover, DIC concentrations match the reactor experiments which were closed to atmospheric CO_2, aside from that dissolved in the fluid or present in the headspace at the beginning of the experiment.

While not present in measurable amounts in either core sample, gypsum, barite, and celestine are all common accessory minerals found as precipitates in FPW (Paukert Vankeuren et al., 2017; Flynn et al., 2019). Barite and celestine are both of particular interest for the oil and gas industry as they can form unwanted scale on equipment or in downhole fissures when sulfate rich formation water is present (Dyer and Graham, 2002; Paukert Vankeuren et al., 2017; Zhang et al., 2017; Krumgalz, 2018; Li et al., 2019; Li et al., 2020; Xiong et al., 2020). The sulfate here could be sourced from the oxidization of pyrite (Harrison et al., 2017), or from sulfur-containing water used to make up the drilling mud or HFF during hydraulic fracturing, or as a degradation product of HFF additives (such as ammonium persulfate). As the concentration of aqueous Fe(II) was below the detection limit for all experiments, the SI relationship for pyrite was not calculated. Although only detected using XRD in the outcrop sample, gypsum is a common accessory mineral that forms as the result of oxidative weathering of pyrite in the presence of calcium bearing minerals (e.g., calcite); therefore, it would be reasonable to hypothesize that gypsum could potentially form during the experiments or hydraulic fracturing. Gypsum and anhydrite ($CaSO_4$) are both Ca sulfate minerals having a maximum solubility of approximately 0.02 mol/L between 25 and 50 °C (Krumgalz, 2018). In all experiments, and in FPW samples, the SI values of both gypsum (Fig. 5i-l), and anhydrite (Fig. S6e-h) indicate these phases are undersaturated and should dissolve (Meijer and Van Rosmalen, 1984; Hörbrand et al., 2018). In contrast with quartz and calcite, gypsum and anhydrite saturation showed a lag in the kinetics during the NaCl experiments, which is likely a product of the kinetics lag in aqueous sulfate concentrations from pyrite dissolution observed in the aqueous chemistry (Azimi, 2010; Fig. 5i-k). This trend was not observed with the FPW samples, with no discernible difference in the calculated SI values for gypsum and anhydrite between the freshwater FPW and RPW FPW (Fig. 5). We believe that this is due to the shut-in period during hydraulic fracturing that allowed the HFF to reach equilibrium with the formation before any wastewater returned from the well.

With their persistent scale-forming potential, significant effort has been invested in determining sources of sulfate, Sr and Ba in FPW, and in elucidating how these minerals nucleate (e.g., Blount, 1974; Zhang et al., 2017; Li et al., 2020; Hakala et al., 2021). As the reactor experiments did not include formation water or sulfate-rich source waters, they are useful in determining whether barite is derived from the formation or occurs as an authigenic precipitate from FPW as proposed by Flynn et al. (2019). In both FPW samples, barite and celestine were close to equilibrium, with their SI values plateauing around ± 0.2 and -0.5, respectively, with minimal difference in SI values calculated for freshwater FPW and RPW FPW (<0.5) (Fig. 5p and t). In the core reactor experiments, the SI values for barite closely resembled those of the corresponding FPW. In order to assess the role temperature played on the SI of barite, we compared the saturation index of barite in FPW at the three experimental temperatures (25 °C, 95 °C, and 140 °C) with the SI of barite SI calculated from the outcrop experiments at the same temperatures. The trends with increasing temperature are opposite, indicating the kinetics of release in the outcrop experiments lag the FPW with respect to barite saturation (Fig. 5s,t). Calculated SI values for celestine show that it is largely undersaturated, although in all freshwater experiments it appears to be approaching that of the SI of both FPW samples. Similar to gypsum, ionic strength and temperature had an

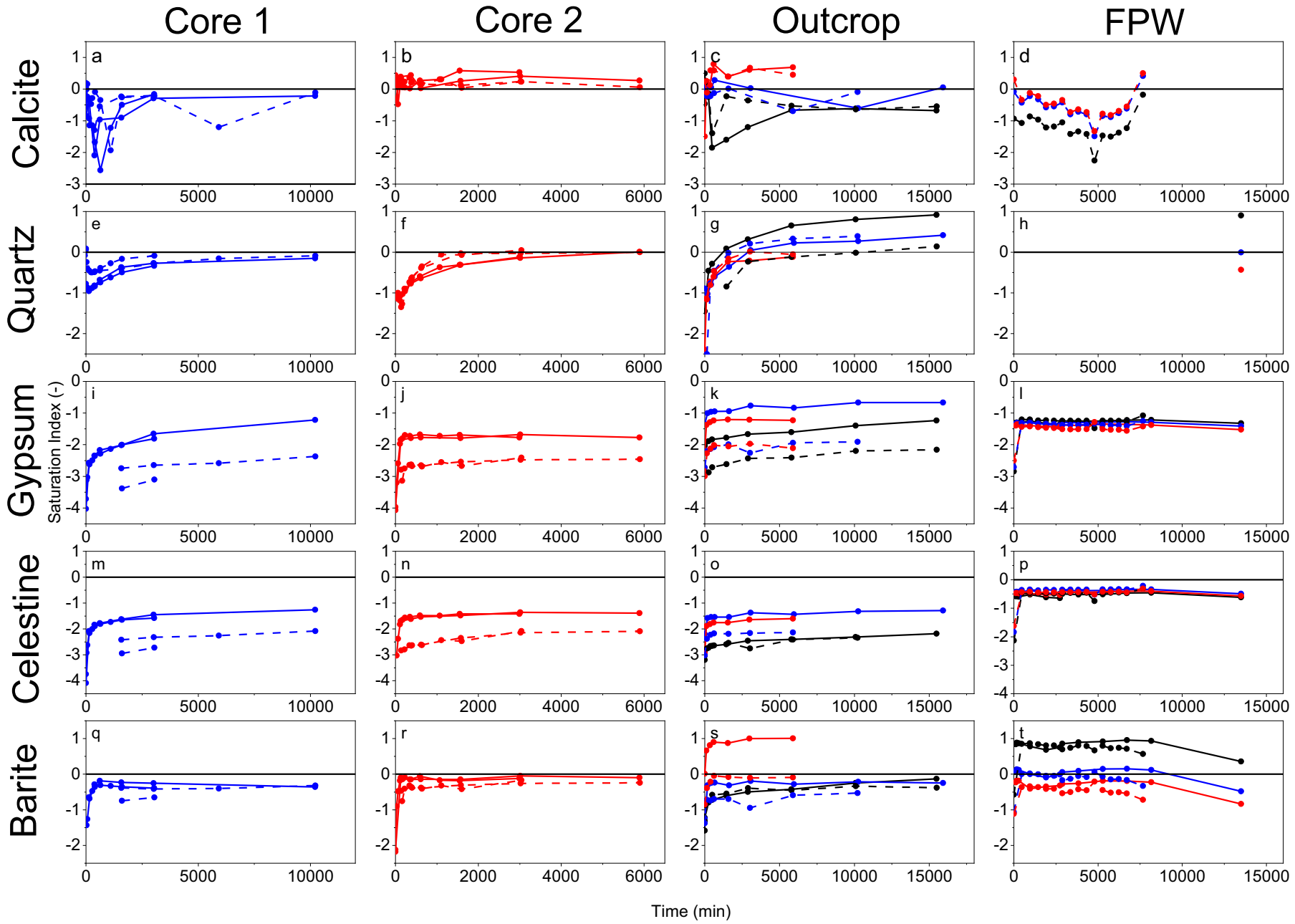

Fig. 5. Saturation indices of calcite (a-d), quartz (e-h), gypsum (i-l), barite (m-p), and celestine (q-t), for experiments with Core 1 (a, e, i, m, q), Core 2 (b, f, j, n, r), Outcrop (c, g, k, o, s), and FPW (d, h, l, p, t). Saturation indices were calculated at experimental temperatures of 25 °C (black), 95 °C (blue), and 140 °C (red), for freshwater (solid) and NaCl/RPW (dashed) experiments. Additional SI are reported in Fig. S4. (For interpretation of the references to colour in this figure legend, the reader is referred to the web version of this article.)

observable effect on the SI of celestine in the reactor experiments that was not observed in the FPW samples (Fig. 5m-p). This result points to the possibility that the aqueous Sr in the FPW samples did not come solely from the dissolution or leaching from the formation. This finding agrees with Owen et al. (2020) who showed that both ion exchange and formation water mixing with HFF were required to accurately model the observed Sr concentrations in FPW. As the barite SI remained around equilibrium in both FPW samples, it would follow that it precipitated during or after hydraulic fracturing, which is what is observed in FPW precipitates from the same formation (Flynn et al., 2019), as well as others (Li et al., 2019).

In summary, the calculated SI values from reactor experiments with the core material more closely match the FPW than the elemental concentrations. In most cases, the pure water experiments correlate well with the SI values from the freshwater FPW. Despite the higher concentrations of most elements reported in the RPW FPW, the SI values from the 0.5 M NaCl experiments were found to be poor proxies (e.g., in the cases of celestine and gypsum). It may be that there is sufficient formation water so that when HFF mixes with it, the resulting FPW becomes saturated with Na and Cl. In effect, the final ionic strength of FPW is not significantly different when either freshwater or RPW are used, and only differs during the first few hours of flowback. In our experiments, barite is near equilibrium, (SI of −0.4 to −0.1 for freshwater experiments and − 0.7 to −0.1 for NaCl experiments) and so the prevalent issue of barite scaling during hydraulic fracturing can be explained primarily by interactions between the rock and source water.

4.2. Environmental implications

Many of the SI calculated from our experiments match with those of FPW, suggesting that formation minerals were the source of many of the components found in solution, particularly Si, Ca, Ba, Sr, DIC, and SO_4. Conversely, Na and Cl are more likely sourced from formation water or HFF. There was also substantial leaching of other trace elements from the formation, including additional PTHM. The concentrations of Sr and Ba, as well as other elements (B, Mg, Si, K, S, Ca, Mo, As, and U) increased with the higher ionic strength of the simulated HFF by reducing the SI of their associated minerals (Tables S8 and S9). In some cases, the salting-in effect was sufficient to increase the concentrations in the reactor experiments to above those of the Canadian Council of Ministers of the Environment (CCME) guidelines. Given the lower water-rock ratio of the reactor experiments compared to actual hydraulic fracturing operations, this could lead to a greater leaching of PTHM from the formation. For example, the CCME guidelines for aquatic life in freshwater systems for As is 5 μg/L or 0.067 μmol/L (CCME, 1997), which was exceeded in all the reactor experiments conducted in 0.5 M NaCl, with an increase of up to 900% from the freshwater experiments (Table 1). If this relationship holds true for hydraulic fracturing, the potential increased As concentration could be up as much as 900% in a well using a higher ionic strength solution (RPW FPW for example) compared to a well using only freshwater as its source water. Consistently across both the cores and the outcrops, and across nearly all temperatures, the salting in effect was greatest for Ba, up to 1870%, indicating a higher salinity could exacerbate the barite-scaling problems associated with hydraulic fracturing (Table 1). While the results from this study indicate that hydraulic fracturing fluid-formation rock interactions to be significant contributors to FPW chemistry from the Duvernay Formation, this may not apply to other reservoirs, such as the Marcellus Formation (Phan et al., 2020; Tieman et al., 2020).

5. Conclusions

The purpose of this study was to determine if laboratory reactor systems can be used to understand the mechanisms and sources of elements leached during hydraulic fracturing into FPW, and if those results can be scaled to field-scale problems. The reactor apparatuses developed here are an adequate way to generate real-time geochemical data on the partitioning of metals during hydraulic fracturing and can be applied to commercial scale problems in hydraulic fracturing, such as the leaching of PTHM and presence of barite scaling. The systems also revealed the role of formation water in the geochemical interactions that result in the composition of FPW. Assuming the necessary conditions are met, such as using a well-mixed core sample from the area of study and using a temperature appropriate for the depth of the reservoir, this method can adequately predict the order of mineral precipitation and the relative rates of metal leaching. Our study, with a primary focus on methodology, provides room to expand the work conducted with the reactors to a variety of problems, such as the effects of organic compounds typically found in HFF on the leachability of metals from the formations. The role of organic compounds has already begun to be explored by assessing the degradation rates and patterns of numerous compounds, such as benzoic acid, ethyl acetate, glutaraldehyde, polyacrylamide, and propylene carbonate (Tasker et al., 2016; Sumner and Plata, 2018; Xiong et al., 2018), but their effect on the leaching of metals has not been well documented. While these studies, and others such as those of Harrison et al. (2017), Jew et al. (2017), Li et al. (2019), and Li et al. (2020), have begun to systematically explore water-rock-fracturing-fluid interactions, many questions remain because of the variability in fracturing fluid chemistry, inter-formation compositional differences and heterogeneity within a single formation. The reactor approach developed here promises to provide new insights into the role of organic compounds – both HFF additives and those native to formations – in the geochemical profile of FPW.

Table 1
The percent increase in leached elements during 0.5 M NaCl experiments in comparison to pure water experiments.

Element	Outcrop 25 °C	Outcrop 95 °C	Outcrop 140 °C	Core 1 I 95 °C	Core 1 II 95 °C	Core 2 I 140 °C	Core 2 II 140 °C
B	5.53	163	223	61.4	−45.9	181	83.5
Mg	20.7	4.00	75.2	55.8	88.8	114.	138
Si	−73.7	32.1	75.5	65.6	−1.49	41.2	3.18
K	54.9	65.1	31.0	35.4	44.64	81.5	49.6
S	33.1	−39.2	34.8	−65.6	−54.8	91.7	60.5
Ca	59.2	−23.1	84.4	50.81	58.98	163	150
As	BDL	486	101	939	226	139	−10.33
Sr	BDL	14.8	284	135	155	165	178
Mo	5.67	31.0	8.12	382	380	8.16	−14.3
Ba	1200	377	1380	1870	1190	1130	998
U	217	493	676	BDL	BDL	BDL	BDL

BDL = below detection limit in either pure water or 0.5 M NaCl experiments, or both.
All values are reported as a percentage, and negative values indicate a smaller concentration of an element in the 0.5 M NaCl experiment as compared to pure water experiments.

Declaration of Competing Interest

The authors declare that they have no known competing financial interests or personal relationships that could have appeared to influence the work reported in this paper.

Acknowledgements

This work was supported by a Natural Sciences and Engineering Research Council of Canada (NSERC) Collaborative Research and Development grant to D.S.A (CRDPJ-469308-14) and NSERC Discovery grants to D.S.A (RGPIN-2020-05289), K.O.K (RGPIN-165831), M.K.G, and S.A.W. (RGPIN-04368/RGPAS-00064). Core material was provided by the Alberta Core Research Center. Outcrop samples were collected from Jasper National Park, AB with the permission of Parks Canada (Permit # JNP-2018-28120). We also would like to thank the contributions of Christopher Noyahr and Paul Sherk, who provided the downhole temperature corrections for the cores used in this study and assisted in the development of illustrations. We also thank the two anonymous reviewers for their insightful comments and feedback.

Appendix A. Supplementary data

Supplementary data to this article can be found online at https://doi.org/10.1016/j.chemgeo.2022.120718.

References

Abualfaraj, N., Guarian, P.L., Olson, M.S., 2014. Characterization of marcellus shale flowback water. Environ. Eng. Sci. 31 (9), 514–524.

AER (Alberta Energy Regulator), 2019. Hydraulic Fracturing. Retrieved from. https://www.aer.ca/protecting-what-matters/holding-industry-accountable/industry-performance/hydraulic-fracturing-water-use (on April 2, 2020).

Alessi, D.S., Zolfaghari, A., Kletke, S., Gehman, J., Allen, D.M., Goss, G.G., 2017. Comparative analysis of hydraulic fracturing wastewater practices in unconventional shale development: Water sourcing, treatment, and disposal practices. Can. Water Resour. J. 42 (2), 105–121.

Arthur, J.D., Bohm, B., Layne, M., 2008. ALL Consulting. Hydraulic Fracturing Considerations for Natural Gas Wells of the Marcellus Shale. Presented at the GWPC Annual Forum in Cincinnati, OH. September 2008.

Azimi, G., 2010. Evaluating the Potential of Scaling due to Calcium Compounds in Hydrometallurgical Processes [PhD. Dissertation]. University of Toronto (156p).

Barth-Naftilan, E., Aloysius, N., Saiers, J.E., 2015. Spatial and temporal trends in freshwater appropriation for natural gas development in Pennsylvania's Marcellus Shale Play. Geophys. Res. Lett. 42 (15), 6348–6356.

Birdwell, J.E., 2017. Development of new shale geochemical reference materials: results from Boquillas Shale interlaboratory testing and other status updates. In: GSA Annual Meeting in Seattle Washington, USA, 69–8. https://gsa.confex.com/gsa/2017AM/webprogram/Paper304400.html (on July 9, 2019).

Bish, D.L., Howard, S.A., 1988. Quantitative phase analysis using the Rietveld method. J. Appl. Crystallogr. 21, 86–91.

Blount, C.W., 1974. Synthesis of barite celestine, anglesite, witherite, and strontianite from aqueous solutions. Am. Mineral. 59, 1209–1219.

CAPP (Canadian Association of Petroliam Producers), 2018. Water Use for Hydraulic Fracturing in Alberta. (Report No. 2018–0033). Retrieved from. https://www.capp.ca/publications-and-statistics/publications/322611.

CCME (Canadian Council of Ministers of the Environment), 1997. Appendix XXII – Canadian water quality guidelines: Updates (June 1997), arsenic, bromacil, carbaryl, chlorpyrifos, deltamethin, and glycols. In: Canadian Water Quality Guidelines, Canadian Council of Resource and Environment Ministers, 1987 (Prepared by the Task Force on Water Quality Guidelines).

Cheary, R.W., Coelho, A., 1992. A fundamental parameters approach to X-ray line-profile fitting. J. Appl. Crystallogr. 25, 109–121.

Delompré, P.L.M., Blewett, T.A., Snihur, K.N., Flynn, S.L., Alessi, D.S., Glover, C.N., Goss, G.G., 2019. The osmotic effect of hyper-saline hydraulic fracturing fluid on rainbow trout, *Oncorhynchus mykiss*. Aquat. Toxicol. 211, 1–10.

Dyer, S.J., Graham, G.M., 2002. The effect of temperature and pressure on oilfield scale formation. J. Pet. Sci. Eng. 35, 95–107.

Flynn, S.L., von Gunten, K., Warchola, T., Snihur, K., Forbes, T.Z., Goss, G.G., Gingras, M. K., Konhauser, K.O., Alessi, D.S., 2019. Characterization and implications of solids associated with hydraulic fracturing flowback and produced water from the Duvernay Formation, Alberta, Canada. Environ Sci Process Impacts 21, 242–255.

Folkerts, E., Goss, G.G., Blewett, T.A., 2020. Investigating the potential toxicity of hydraulic fracturing flowback and produced water spills to aquatic animals in freshwater environments: a North American perspective. In: Reviews of Environmental Contamination and Toxicology (Continuation of Residue Reviews). Springer, Cham, pp. 1–56.

Gallegos, T.J., Varela, B.A., Haines, S.S., Engle, M.A., 2015. Hydraulic fracturing water use variability in the United States and potential environmental implications. Water Resour. Res. 51 (7), 5839–5845.

Goss, G.G., Alessi, D.S., Gehman, J., Allen, D., Brisbois, J., Kletke, S., Zolfaghari, A., Notte, C., Thompson, D.Y., Hong, K., Junes, V.R.C., de Araujo, W.B.G., Prosser, C., 2015. A Comparative Review and Analysis of Hydraulic Fracturing Wastewater Management Practices Across Four North American Basins. Canandian Water Network, p. 189. http://www.cwn-rce.ca/project-library.

Hackley, P.C., Cardott, B.J., 2016. Application of organic petrography in north American shale petroleum systems: a review. Int. J. Coal Geol. 163, 8–51.

Hakala, J.A., Paukert Vankeuren, A.N., Scheuermann, P.P., Lopano, C., Guthrie, G.D., 2021. Predicting the potential for mineral scale precipitation in unconventional reservoirs due to fluid-rock and fluid mixing geochemical reactions. Fuel 284, 118883.

Harrison, A.L., Jew, A.D., Dusting, M.K., Thomas, D.L., Joe-Wang, C.M., Barger, J.R., Johnson, N., Brown, G.E., Maher, K., 2017. Element release and reaction-induced porosity alteration during shale-hydraulic fracturing fluid interactions. Appl. Geochem. 82, 47–62.

He, Y., Flynn, S.L., Folkerts, E., Zhang, Y., Ruan, D., Alessi, D.S., Martin, J.W., Goss, G.G., 2017. Chemical and toxicological characterizations of hydraulic fracturing flowback and produced water. Water Res. 114, 78–87.

Hill, R.J., Howard, C.J., 1987. Quantitative phase analysis from neutron powder diffraction data using the Rietveld method. J. Appl. Crystallogr. 20, 467–474.

Hörbrand, T., Baumann, T., Moog, H.C., 2018. Validation of hydrogeochemical databases for problems in deep geothermal energy. Geotherm. Energy 6 (2) (30pp).

Jew, A.D., Dustin, M.K., Harrison, A.L., Joe-Wang, C.M., Thomas, D.L., Maher, K., Brown Jr., G.E., Bargar, J.R., 2017. Impact of organics and carbonates on the oxidation and precipitation of iron during hydraulic fracturing of shale. Energy Fuel 31, 3643–3658.

Krumgalz, B.S., 2018. Temperature dependence of mineral solubility in water. Part 3. Alkaline and alkaline earth sulfates. J. Phys. Chem. Ref. 47, 023101 (30pp).

Li, Q., Jew, A.D., Kohli, A., Maher, K., Brown Jr., G.E., Bargar, J.R., 2019. Thickness of chemically altered zones in shale matrices resulting from interactions with hydraulic fracturing fluid. Energy Fuel 33, 6878–6889.

Li, Q., Jew, A.D., Brown Jr., G.E., Bargar, J.R., Maher, K., 2020. Reactive transport modeling of shale-fluid interactions after imbibition of fracturing fluids. Energy Fuel 34, 5511–5523.

Locock, A.J., Chesterman, D., Caird, D., Duke, M.J.M., 2012. Miniaturization of mechanical million for powder X-ray diffraction. Powder Diffract. 27, 189–193.

Mehler, W.T., Nagel, A., Flynn, S., Zhang, Y., Sun, C., Martin, J., Alessi, D., Goss, G.G., 2020. Understanding the effects of hydraulic fracturing flowback and produced water (FPW) to the aquatic vertebrate, *Lumbriculus variegatus* under various exposure regimes. Environ. Pollut. 259, 113889.

Meijer, J.A.M., Van Rosmalen, G.M., 1984. Solubilities and supersaturations of calcium sulfate and its hydrates in seawater. Desalination 51, 255–305.

Morey, G.W., Fournier, R.O., Rowe, J.J., 1962. The solubility of quartz in water in the temperature interval from 25° to 300°C. Geochim. Cosmochim. Acta 26, 1029–1043.

Owen, J., Bustin, R.M., Bustin, A.M.M., 2020. Insights from mixing calculations and geochemical modeling of Montney Formation post hydraulic fracturing flowback water chemistry. J. Pet. Sci. Eng. 195, 107589 (18pp).

Parkhurst, D., Appelo, C.A.J., 2013. PHREEQC (Version 3) -A Computer Program for Speciation, Batch Reaction, One-Dimensional Transport, and Inverse Geochemical Calculations. US Geologic Survey, Water Resources Division, Denver, CO.

Paukert Vankeuren, A.N.P., Hakala, J.A., Jarvis, K., Moore, J.E., 2017. Mineral reactions in shale gas reservoirs: barite scale formation from reusing produced water as hydraulic fracturing fluid. Environ. Sci. Technol. 51, 9391–9402.

Phan, T.T., Hakala, J.A., Sharma, S., 2020. Appliation of geochemical signals in unconventional oil and gas reservoir produced waters towards charaxterizing in situ geochemical fluid-shale reactions. Sci. Total Environ. 714, 136867.

Rietveld, H., 1969. A profile refinement method for nuclear and magnetic structures. J. Appl. Crystallogr. 2, 65–71.

Rosenbauer, R.J., Koksalan, T., Palandri, J.L., 2005. Experimental investigation of CO_2-brine-rock interactions at elevated temperatures and pressure: Implications for CO_2 sequestration in deep-saline aquifers. Fuel Process. Technol. 86 (14–15), 1581–1597.

Rowan, E.L., Engle, M.A., Kraemer, T.F., Schroeder, K.T., Hammack, R.W., Doughten, M. W., 2015. Geochemical and isotopic evolution of water produced from Middle Devonian Marcellus shale gas wells, Appalachian basin, Pennsylvania. AAPG Bull. 99, 181–206.

Shaffer, D.L., Chavez, L.H.A., Ben-Sasson, M., Castrillón, S.R., Yip, N.Y., Elimelech, M., 2013. Desalination and reuse of high-salinity shale gas produced water: drivers, technologies, and future directions. Environ. Sci. Technol. 47, 9569–9583.

Shen, L., Schmitt, D.R., Haug, K., 2018. Measurements of the States of in Situ Stress for the Duvernay Formation near Fox Creek, west-Central Alberta; Alberta Energy Regulator / Alberta Geological Survey, AER/AGS Report, 97 (29 pp).

Siever, R., 1962. Silica solubility, 0°-200°C, and the diagenesis of siliceous sediments. Geology 70 (2), 127–150.

Sumner, A.J., Plata, D.L., 2018. Exploring the hydraulic fracturing parameter space: a novel high-pressure, high-throughput reactor system for investigating subsurface chemical transformations. Environ Sci Process Impacts 20, 318–331.

Sun, Y., Want, D., Tsang, D.C.W., Wang, L., Ok, Y.S., Feng, Y., 2019. A critical review of risks, characteristics, and treatment strategies for potentially toxic elements in wastewater from shale gas extraction. Environ. Int. 125, 452–469.

Tasker, T.L., Piotrowski, P.K., Dorman, F.L., Burgos, W.D., 2016. Metal associations in marcellus shale and fate of synthetic hydraulic fracturing fluids reacted at high pressure and temperature. Environ. Eng. Sci. 33 (10), 753–765.

Taylor, R.S., Stobo, B., Niebergall, G., Aguilera, R., Walter, J., Hards, E., 2014. Optimization of Duvernay fracturing treatment design using fully compositional dual permeability numeric reservoir simulations. In: SPE/CSUR Unconventional Resources Conference. Society of Petroleum Engineers, Canada.

Tieman, Z.G., Stewart, B.W., Capo, R.C., Phan, T.T., Lopano, C.L., Hakala, J.A., 2020. Barium isotopes track the source of dissolved solids in produced water from the unconventional Marcellus Shale gas play. Environ. Sci. Technol. 54, 4275–4285.

Wang, Y., von Gunten, K., Bartova, B., Meisser, N., Astner, M., Burger, M., Bernier-Latmani, R., 2016. Products of in situ corrosion of depleted uranium ammunition in bosnia and herzegovina soils. Environ. Sci. Technol. 50, 12266–12274.

Wilson, M.A., Burt, R., Lee, C.W., 2006. Improved elemental recoveries in soils with heating boric acid following microwave total digestion. Commun. Soil Sci. Plant Anal. 27 (3–4), 513–524.

Xiong, B., Miller, Z., Roman-White, S., Tasker, T., Farina, B., Piechowicz, B., Burgos, W. D., Joshi, P., Zhu, L., Gorski, C.A., Zydney, A.L., Kumar, M., 2018. Chemical degradation of polyacrylamide during hydraulic fracturing. Environ. Sci. Technol. 52, 327–336.

Xiong, W., Gill, M., Moore, J., Crandall, D., Hakala, J.A., Lopano, C., 2020. Influence of reactive flow conditions on barite scaling in marcellus shale during stimulation and shut-in periods of hydraulic fracturing. Energy Fuel 34 (11), 13625–13635.

Zhang, F., Dai, Z., Yan, C., Bhandari, N., Yan, F., Liu, Y., Zhang, Z., Ruan, G., Kan, A.T., Tomson, M.B., 2017. Barite-scaling risk and inhibition at high temperature. Soc. Pet. Eng. 22 (1), 69–79.

Zhong, C., Li, J., Flynn, S.L., Nesbø, C.L., Sun, C., von Gunten, K., Lanoil, B.D., Goss, G.G., Martin, J.W., Alessi, D.S., 2019. Temporal changes in microbial community composition and geochemistry in flowback and produced water from the duvernay formation. ACS Earth Space Chem. 3, 1047–1057.

Ziemkiewicz, P.F., He, Y.T., 2015. Evolution of water chemistry during Marcellus Shale gas development: a case study in West Virginia. Chemosphere 134, 224–231.